Naval Research Laboratory

Washington, DC 20375-5320

Blast Mitigation by Water Mist
(1) Simulation of Confined Blast Waves

Douglas Schwer
K. Kailasanath

Center for Reactive Flow and Dynamical Systems
Laboratory for Computational Physics and Fluid Mechanics

August 16, 2002

20021016 195

REPORT DOCUMENTATION PAGE

Form Approved
OMB No. 0704-0188

1. REPORT DATE (DD-MM-YYYY)	2. REPORT TYPE	3. DATES COVERED (From - To)
August 16, 2002	Memorandum Report	

4. TITLE AND SUBTITLE	5a. CONTRACT NUMBER
Blast Mitigation by Water Mist (1) Simulation of Confined Blast Waves	**5b. GRANT NUMBER** 64-1530-02
	5c. PROGRAM ELEMENT NUMBER

6. AUTHOR(S)	5d. PROJECT NUMBER
	5e. TASK NUMBER
Douglas Schwer and K. Kailasanath	**5f. WORK UNIT NUMBER**

7. PERFORMING ORGANIZATION NAME(S) AND ADDRESS(ES)	8. PERFORMING ORGANIZATION REPORT NUMBER
Naval Research Laboratory, Code 6410 4555 Overlook Avenue, SW Washington, DC 20375-5320	NRL/MR/6410--02-8636

9. SPONSORING / MONITORING AGENCY NAME(S) AND ADDRESS(ES)	10. SPONSOR / MONITOR'S ACRONYM(S)
	11. SPONSOR / MONITOR'S REPORT NUMBER(S)

12. DISTRIBUTION / AVAILABILITY STATEMENT

Approved for public release; distribution is unlimited.

13. SUPPLEMENTARY NOTES

14. ABSTRACT

Effectively minimizing the damage due to onboard explosions and blast waves on naval ships has always been a priority to the Navy. With recent events and the war on terrorism, this need has become important to a much broader base of people to help protect platforms and infrastructure. Water presents a flexible, cost-effective, and clean method for mitigating the effects of the blast wave and has received much attention recently from experimentalists. There is, however, only limited understanding on exactly how to use water most effectively to mitigate blasts. The purpose of this research is to clarify issues related to how water can be used to mitigate blasts within enclosures, and specifically looks at the use of water mist in mitigating blast waves.

A parallel, FCT-based simulation technique was developed to examine initial blast properties and long-term pressure development in enclosures for TNT explosions. The simulation technique uses a simplified approach to modeling the area immediately surrounding the explosive (defined as the "blast" volume), avoiding a costly detonation calculation for the initial explosive. Simulations show that accurate predictions of the initial gas overpressure away from the "blast" volume can be made with a one-dimensional spherically symmetric model. The one-dimensional solutions do not adequately capture the long-term pressure development within the enclosure. Instabilities in the contact discontinuity that require multi-dimensional simulations become important in driving the secondary fireball reactions for TNT. Axisymmetric simulations are shown to be adequate in reproducing the long-term overpressure development in enclosures.

15. SUBJECT TERMS

Blast mitigation; Damage control; Water-mist suppression; Shock suppression; Explosions; Modeling and simulation

16. SECURITY CLASSIFICATION OF:			17. LIMITATION OF ABSTRACT	18. NUMBER OF PAGES	19a. NAME OF RESPONSIBLE PERSON
a. REPORT	**b. ABSTRACT**	**c. THIS PAGE**	UL	25	Douglas Schwer
Unclassified	Unclassified	Unclassified			**19b. TELEPHONE NUMBER** (include area code) (202) 767-3615

Standard Form 298 (Rev. 8-98)
Prescribed by ANSI Std. Z39.18

Contents

List of Tables

List of Figures

BLAST MITIGATION BY WATER MIST
(1) SIMULATION OF CONFINED BLAST WAVES

1   Introduction

Explosions and fires have always represented a danger to naval ships. Large amounts of fuel and ordnance onboard these ships provide plentiful fuel for explosions and fires even in peacetime. Recent events such as the USS Cole have highlighted the need to be able to mitigate the effects of explosions on board ships, whether caused by internal or external factors.

Several recent studies have looked at water to mitigate the effects of explosions. Using water is attractive for several reasons. The large heat capacity and latent heat of vaporization allows water to easily absorb a large amount of energy. In addition, water systems have a great deal of flexibility and low cost, are environmentally safe and clean to use, and can serve a dual role in fire suppression in peacetime situations and explosion mitigation during war and terrorist situations.

Water mist is currently being developed as a fire suppression tool on naval ships to replace the Halon systems currently employed [1]. Because of this, much effort has gone into developing water mist spray systems, characterizing the resulting spray and its effect on the fire. A considerable amount of research has also been accomplished with respect to water suppression of explosions (for a review see [2]). Although water mist systems also appear attractive for blast mitigation, there are still several issues that need to be addressed pertaining to characteristics of explosions on board ships and mitigating them [2-4]. Many of these questions eventually need to be addressed through experiments and testing. However, modeling can help substantially reduce the number and total cost of experiments, and provide insight into the mechanisms that are important for blast mitigation. This specific memo report addresses modeling of TNT explosions within confined spaces. TNT was chosen because it is a fairly common and well understood explosive. Because it is under-oxidized, correctly simulating the blast and quasi-static pressure also requires modeling the fireball that results from the oxidation of unburned carbon and carbon monoxide. The techniques employed here are not specific to TNT, however, and should carry over to other explosives without difficulties.

In terms of blast mitigation, our main interest is obtaining correct initial overpressure and quasi-static pressure away from the initial charge. Because of this, we use a fairly simple model near the charge, where the physics is very complex, and a more accurate calculation away from the charge, where the physics is much simpler. For this report, we look at two reference cases, a spherical enclosure and a cylindrical enclosure, such that the volumes of both are 3.25×10^7 cm^3. The blast is created by 2.12 kg (4.67 lbs) of TNT exploded in the center of the enclosure.

2   Modeling of TNT Blast Waves in Enclosures

The chemical structure of TNT is $C_7H_5N_3O_6$. TNT is extremely oxygen deficient, thus it requires excess oxygen in order to react completely. Without excess air, TNT will form the following products [5]:

$$C_7H_5N_3O_6 \rightarrow 2.5\ H_2O + 3.5\ C(s) + 3.5\ CO + 1.5\ N_2 + 247\ \text{kcal/mol TNT}$$
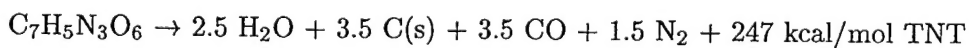
where water is assumed to be in gaseous form. For a typical explosion into air with excess oxygen,

the C(s) is first converted to CO and then the CO is converted to CO_2 within the blast front. For every mole of explosive, 5.25 moles of O_2 are required in order to fully oxidize the C(s) and CO molecules.

$$3.5 \text{ C(s)} + 3.5 \text{ CO} + 5.25 \text{ O}_2 \rightarrow 7 \text{ CO}_2 + 567 \text{ kcal/mol TNT}$$
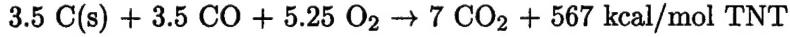
This last reaction could also be divided into two steps: the solid carbon is converted to CO, and then the CO is converted to CO_2. As indicated by the heat of reaction, much of the energy for a TNT blast is produced in the secondary fireball. Because of this, and also because the fireball encompasses a fairly large region, it is important to model this reaction process within the blast front. The initial blast, on the other hand, is confined to a fairly small region.

The radius required to consume all of the C(s) and CO to form CO_2 from the initial blast is called the fireball radius for an explosive. For the base case of 2.12 kg TNT exploding into a container filled with air at standard temperature and pressure, the fireball radius is 111 cm (volume 5.729×10^6 cm^3). It is important to note that the above radius really only has meaning for quasi-steady constant volume calculations. That is, if you explode TNT in a spherical container with a radius of 111 cm, there is enough oxygen within the container to totally convert the C(s) and CO to CO_2. This does *not* mean that all of the initial CO and C(s) will be consumed in the initial blast by 111 cm, because that would require the oxygen to fully mix with the C(s) and CO. In fact, because the fuel only slowly mixes with the oxygen at the contact discontinuity, reactions will continue much further out than the "fireball radius."

The approach used for modeling blasts in enclosures in this report is based on the fact that the volume containing and immediately surrounding the explosive is very small compared to the total volume of the enclosure. Since these simulations focus on the properties of the blast away from the initial explosive, we separate our domain into two regions. The region near the initial explosive charge is defined as the "blast" volume. The initial density, pressure, and temperature are calculated within this volume assuming a constant volume well-stirred reactor calculation that has gone to completion. Initial conditions away from the blast region are set at the ambient conditions. The CFD calculation is started as a bursting-diaphragm problem, where the initial velocity is set to zero everywhere, and at time zero the "diaphragm" separating the "blast" volume from the ambient air is removed and the simulation starts.

2.1 Governing Equations

As mentioned previously, the shock front that forms from the initial blast cannot be treated as a pure gas, because it carries particles of C(s) that are burned to form CO at the contact discontinuity. For purposes of the computations, we treat this as a fine dust that has a very small volume fraction ($\alpha_g \gg \alpha_{C(s)}$), and is in temperature and velocity equilibrium with the gas, similar to the analysis done by Marble for dusty gases [6]. By making these assumptions, we can combine the gas and carbon-dust mass, momentum, and energy equations such that the conservation equations for inviscid flow become:

$$\frac{\partial \rho}{\partial t} + \nabla \cdot \rho \mathbf{u} = 0 \tag{1}$$

$$\frac{\partial \rho \mathbf{u}}{\partial t} + \nabla \cdot \rho \mathbf{u} \mathbf{u} = -\nabla P \tag{2}$$

$$\frac{\partial E}{\partial t} + \nabla \cdot (E + P)\mathbf{u} = 0 \tag{3}$$

where ρ is the total density of the flow ($\rho = \sum_{i=1}^{N_g} \rho_{g,i} + \rho_{C(s)}$). In addition to these conservation equations, we also have additional conservation equations for the gas species and the carbon dust:

$$\frac{\partial \rho_{g,i}}{\partial t} + \nabla \cdot \rho_{g,i}\mathbf{u} = S_{g,i} \tag{4}$$

$$\frac{\partial \rho_{C(s)}}{\partial t} + \nabla \cdot \rho_{C(s)}\mathbf{u} = S_{C(s)} \tag{5}$$

where $S_{g,i}$ and $S_{C(s)}$ are the source terms due to reactions, and will be discussed in more detail below. Because of the complex mixture, we compute the total energy straight from the enthalpy calculation:

$$E = \sum_{i=1}^{N_g} \rho_{g,i} h_{g,i}(T) + \rho_{C(s)} h_{C(s)}(T) - P + \frac{1}{2}\rho u^2 \tag{6}$$

where the species enthalpies $h_i(T)$ are computed from polynomial curve fits given in Appendix A. This representation has the added advantage that we do not have to add energy due to reactions because that is already incorporated into the expression for E. The disadvantage of using this system is we now have to solve a non-linear equation to back out the temperature from the total energy, and is thus much less computationally efficient than the simpler expression commonly used for E in high speed CFD codes. Two global reactions are used to convert the carbon dust and carbon monoxide to carbon dioxide,

$$C(s) + 1/2 \ O_2 \rightarrow CO$$
$$CO + 1/2 \ O_2 \rightarrow CO_2$$
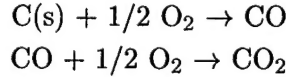
Both reactions are treated as infinitely fast above a temperature of 1000 K. This approximation should be very good given the extreme temperature and pressure conditions occurring within the shock. First we burn C(s) to CO until the supply of C(s) or O_2 is depleted, and then, if there is any excess oxygen, we burn CO to CO_2. The exact expressions for the reaction rate used are:

$$(\Delta t \dot{r}_f) = \min\left[\frac{\rho_f}{W_f}, \frac{2\rho_{O_2}}{W_{O_2}} \right] \tag{7}$$

where f represents either C(s) or CO. The source terms for the species involved in reactions become:

$$S_{C(s)} = \Delta t W_{C(s)} \dot{r}_{C(s)} \tag{8}$$

$$S_{g,O_2} = -1/2\Delta t W_{O_2}\left(\dot{r}_{C(s)} + \dot{r}_{CO} \right) \tag{9}$$

$$S_{g,CO} = \Delta t W_{CO}\left(\dot{r}_{C(s)} - \dot{r}_{CO} \right) \tag{10}$$

$$S_{g,CO_2} = \Delta t W_{CO_2} \dot{r}_{CO} \tag{11}$$

3

To close the system, we need an equation of state to relate the pressure to the temperature. For explosives, the equation of state is often the most important part of the calculation. Since we are interested in the blast solution away from the explosive, we use a fairly simple equation of state, called the Nobel-Able equation of state. This gas law has the form:

$$P = \frac{\rho R T}{1 - an} \tag{12}$$

where a is empirically determined and n is the molar density of the gas. The Nobel-Able gas law accounts for the effect of finite volume molecules in calculating the pressure, and is only valid for moderately high pressures compared to many other equations of states used for explosives. The suggested value for a for TNT explosions is 25 cm^3/mol [7], however, we found a value of 15 cm^3/mol to work much better due to the extreme pressures found initially close to the explosive.

2.2 Initial Conditions

As previously mentioned, the simulation is initialized by defining a "blast" volume where the explosive is expected to react completely in a constant volume, adiabatic process, and then starting the simulation as a broken diaphragm problem. Currently, the volume specified as the blast volume is arbitrarily chosen but is based on the initial explosive radius. For this report, we examine several different blast volume sizes.

The pressure and temperature within the blast volume are calculated assuming a constant volume, adiabatic reaction where the explosive reacts completely with the available oxygen. For this calculation, we used the same thermal properties and equation of state as described above for the simulation. As an example, we show the results from the constant-volume calculation for an initial blast volume of 11.1 cm and a charge of 2.12 kg (4.67 lbs) TNT in Table 1.

An important point to note is that the final gas composition is completely dominated by gases evolved from TNT. Thus, as we change the blast radius, the number of moles and temperature will stay fairly constant; but the ideal gas pressure will increase or decrease as the cube of the ratio of radii, as shown in Table 2.

The pressures, in fact, can quickly become so extreme that the ideal equation of state does not work well (the ideal gas law is a very good approximation up to about 500 atm, although many ballistics scientists use the ideal gas law up to about 2000 atm with only relatively small errors). This would indicate that a blast radius of 14.8 cm is about the smallest radius where the ideal gas law is still reasonable. For smaller blast radii, an accurate equation of state becomes more critical, whereas for larger blast radii, the ideal gas law is adequate.

2.3 Solution Procedure

The solution procedure used for the current simulations is based on the explicit-FCT algorithm [8] extensively used for high speed flows. This method is described in detail in NRL/MR/6410-93-7192 [9], and will not be repeated here for brevity. The scheme uses spatial splitting and also splits the reaction calculation from the convection calculation. Unlike the computations described in the above memorandum report, we use curve-fits for calculating the total energy that are designed to

Table 1: Initial and final conditions for a constant volume explosion of 2.12 kg of TNT. The gas initial conditions represent the gas in the initial "blast" radius, outside of the explosive.

Amount of TNT: 2.12 kg
Mole TNT: 9.334
Volume TNT: 1,285 cm^3

Radius of blast: 11.1 cm
Volume of blast: 5,729 cm^3

Gas Initial conditions:

	Mole	Density (mol/cm^3)
O_2:	0.0489	8.532×10^{-6}
N_2:	0.1838	3.208×10^{-5}
Temperature:	300.0 K	
Pressure:	1.013 bar	
Molar density:	4.061×10^{-5} mol/cm^3	
Molecular weight:	28.85 gm/mol	

Gas Final conditions:

	Mole	Density (mol/cm^3)
O_2:	0	0
N_2:	14.18	2.476×10^{-3}
H_2O:	23.33	4.073×10^{-3}
CO:	32.77	5.720×10^{-3}
CO_2:	0	0
Temperature:	3501 K	
Pressure:	4,376 bar	
Molar density:	12.27×10^{-3} mol/cm^3	
Molecular weight:	24.78	

Mole C(s):   32.57
Density C(s): 5.686×10^{-3} mol/cm^3, 6.829×10^{-2} gm/cm^3

Table 2: Pressure, temperature, and molar density of explosion within a constant volume container of different radii.

Blast radius(cm)	Temp. (K)	Press. (bar)*	Press. (bar)**	Molar density (mol/cm^3)
14.8	3498	1514	1642	5.204×10^{-3}
11.1	3501	3571	4376	1.227×10^{-2}
6.75	3502	15,840	85,990	5.439×10^{-2}

* Ideal gas equation of state
** Nobel-Able equation of state

work with the thermodynamic data in the form used in the NASA chemical equilibrium code [10]. The pressure is calculated by first computing the temperature from the total energy, and then backing out the pressure using the Nobel-Able gas equation of state. This method is computationally expensive, and is only done for these simple calculations to make sure our models are accurate. Other features of the code include a parallel implementation using OpenMP (*www.openmp.org*), the ability of using multi-block rectilinear grids [11], and the ability to put in dispersed phases via an Eulerian sectional approach [12], although none of these are used for the one-dimensional cases, and for this report only the OpenMP option is used for the two-dimensional and three-dimensional cases.

3 Results

The simulations presented in this report are divided into two broad categories. First, we look at the characteristics of the initial blast. This blast will typically be a spherically shaped shock that emanates from the explosive. The overpressures associated with this initial shock are very extreme, but of short duration. The second characteristic we examine which is important for enclosures is the quasi-steady pressure rise. This is the pressure rise due from the initial blast and the oxidation of the remaining C(s) and CO. For mitigation, we are concerned with both the initial blast and the quasi-steady pressure/temperature rise. The majority of computations done for this report have a blast radius of $R_b = 11$ cm.

3.1 Initial blast simulations

The first set of computations examine the initial blast, which is spherical in nature emanating from the explosive. Because of this, for most simulations we used a one-dimensional spherically-symmetric solution procedure to make the computations efficient. The domain was chosen to be 173 cm long, where 111 cm is the secondary fireball radius.

The solution for the base case (2.12 kg TNT, spherical geometry with $r = 173$ cm, 11 cm blast radius, well-resolved) at several instances in time is shown in Figure 1. There are several interesting features of these spherical blasts. The first striking feature of the density (Fig. 1a) and pressure (Fig. 1b) plots are that the high levels of pressure and density fall off rapidly away from the blast

6

volume. The pressure, in particular, quickly reduces from the initial extreme levels. At about 30 cm from the initial "blast" radius, the overpressure has already been reduced to about 45 bar. Similarly, the density, while being extremely high in the initial blast volume, has a maximum within the shock front of around 0.01 gm/cm^3 (compared to the ambient density of 0.00117 gm/cm^3). Behind the shock wave, as time progresses, both the density and the pressure in the original blast volume go below ambient pressure and density due to over-expansion, which also forces the velocity (Fig. 1e) to become negative between the shock front and the original blast volume. For these cases the effect of reactions is seen at the contact surface as a spiked rise in temperature (Fig. 1c), or a decrease in density. The reactions do not occur at the blast front because the air is not premixed, thus there is no coupling of the blast front and the reaction and it is not a detonation wave.

Another interesting result from the simulation is the shock location and shock velocity, as shown in Figure 2. Figure 2b shows that the shock velocity quickly rises as the shock sets up from the initial condition, and then quickly decelerates because of the spherical expansion. The shock overpressure and temperature are shown in Figure 3. The shock overpressure is important because it indicates the maximum pressure experienced at a specific location in the domain. These values can easily be compared with experimental values to validate the numerical procedure (as shown below). The shock temperature is not as useful as the overpressure, because the highest temperatures in the flow usually occur behind the shock at the contact surface, where the carbon dust and CO oxidize. However, this quantity may become important for mitigation purposes.

To ensure the accuracy of our computations, the spatial and temporal resolution requirements to obtain relatively grid-independent solutions are examined. First, four different spatial representations, from 250 cells to 2000 cells in a domain of 173 cm (thus $\Delta x = 0.692$ cm to 0.0815 cm), are computed with a time-step of 0.05 μs. A comparison of solutions at two different spatial resolutions is shown in Figure 4, and the effect of grid resolution on the resulting shock location and overpressure is shown for all resolutions in Figure 5. Interestingly, the lowest resolution (250 cells) has a shock speed much higher than the other three resolutions. Examining the temperature solution (Fig. 4b), we determine that this is caused by the flame at the contact surface effecting the initial shock for the low resolutions. This occurs because there is a much greater degree of mixing between the carbon dust and CO and the oxygen due to numerical diffusion, resulting in more reactions that tend to drive the flow forward. Examining the spatial solution and shock overpressure, there is very little difference between the 1000 and 2000 cell solutions, and only a small difference with the 500 cell solution. The temporal resolution was also investigated, and found to have little effect on the solution.

The next set of results examine the effect of C(s) and CO oxidation on the overall shock system, as shown in Figure 6. For the one-dimensional case, the effect of reactions is minimal. The reactions occur at the contact surface, which is away from the initial shock. The effect of the reactions is to raise the temperature right at the contact surface. It does not, however, effect the temperature elsewhere within the shock, and does not effect the pressure and velocity anywhere in the domain. For the non-reacting case, a slight jiggle in the temperature is seen at the contact surface. This is believed to be caused by the non-linear nature of the FCT solution procedure, such that energy,
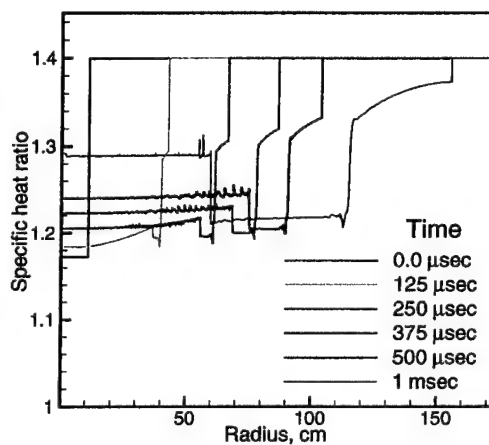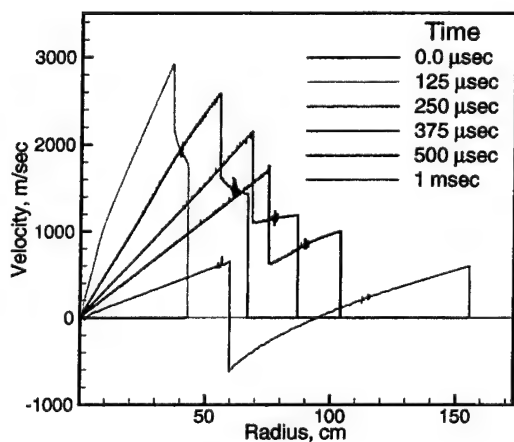
7
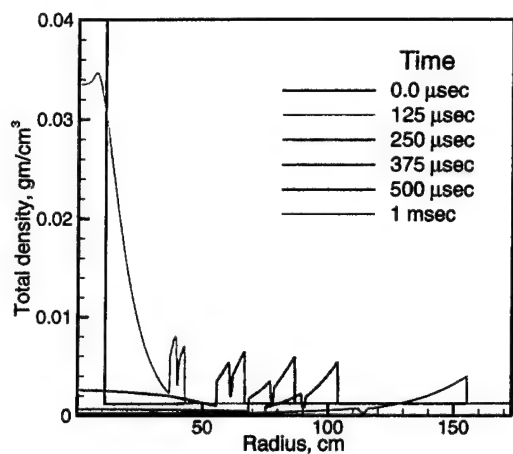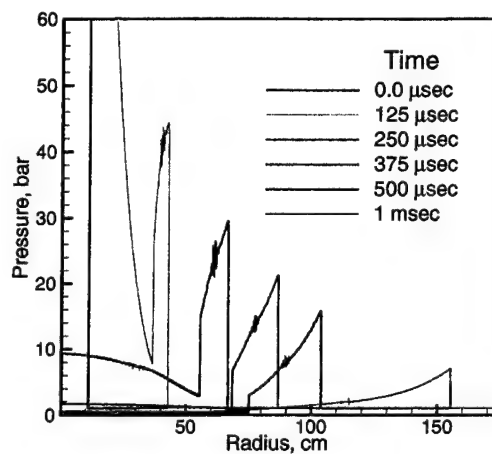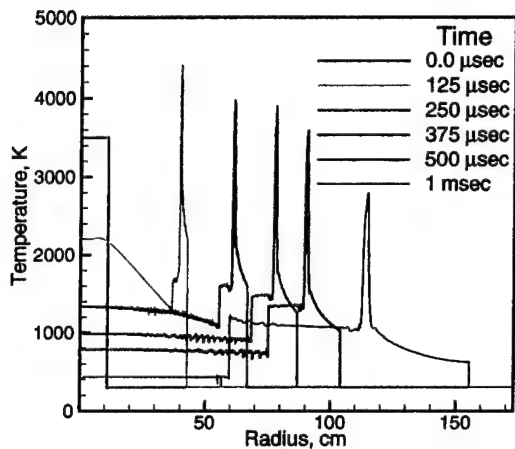
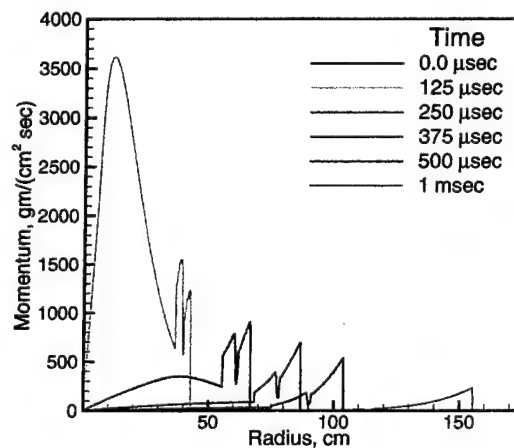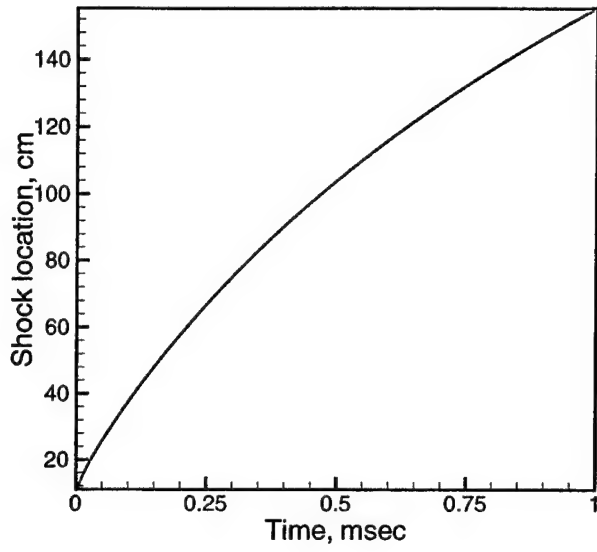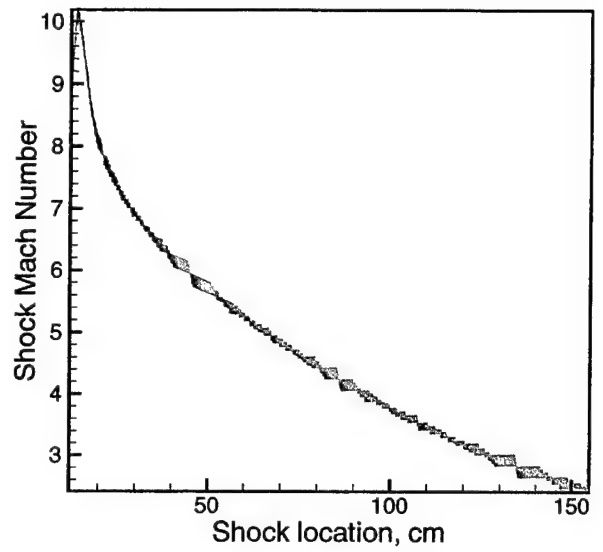Figure 1: Solution from the blast. $R_b = 11$ cm, $W_{TNT} = 2.12$ kg. Cells = 2000. $\Delta t = 0.05$ μs.
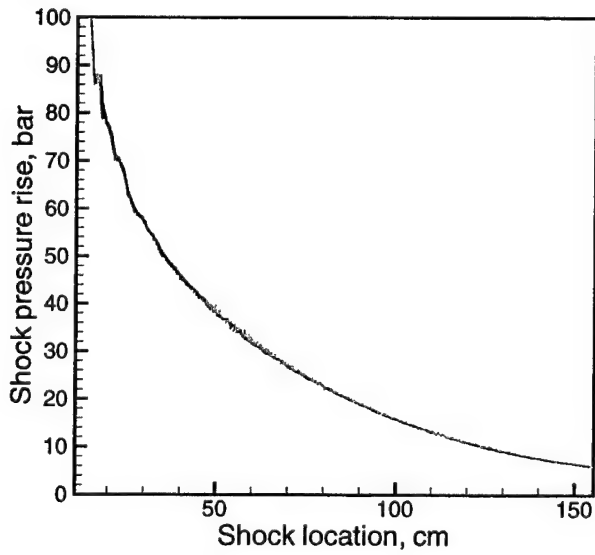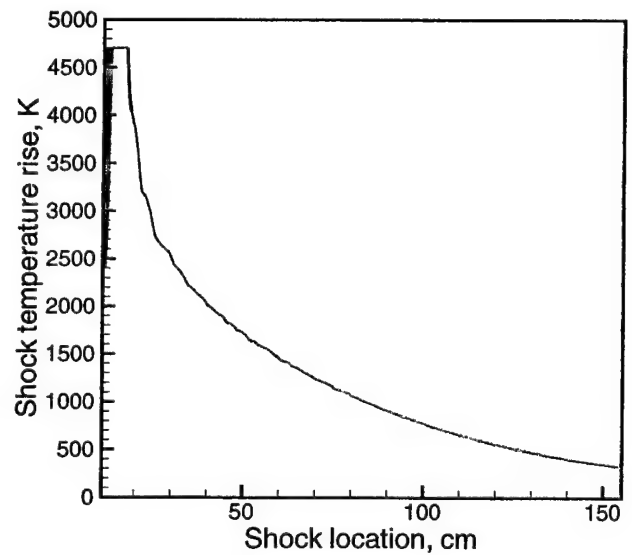
8

Figure 2: Initial shock location (a) and shock speed (b) from the blast. $R_b = 11$ cm, $W_{TNT} = 2.12$ kg. Cells = 2000. $\Delta t = 0.05$ μs.

Figure 3: Initial shock overpressure (a) and temperature rise (b) from the blast. $R_b = 11$ cm, $W_{TNT} = 2.12$ kg. Cells = 2000. $\Delta t = 0.05$ μs.
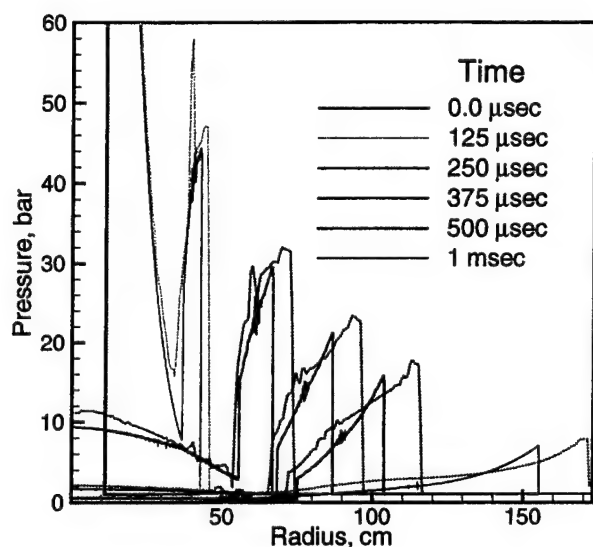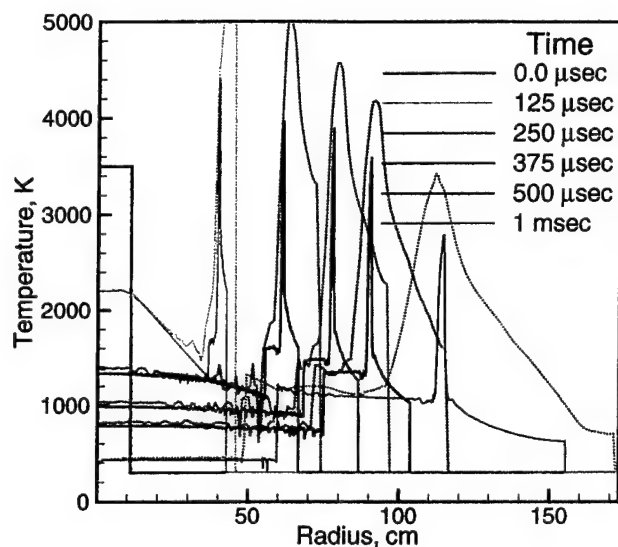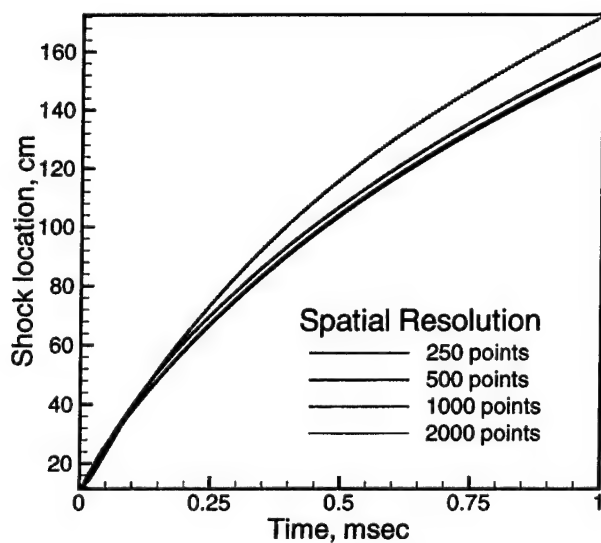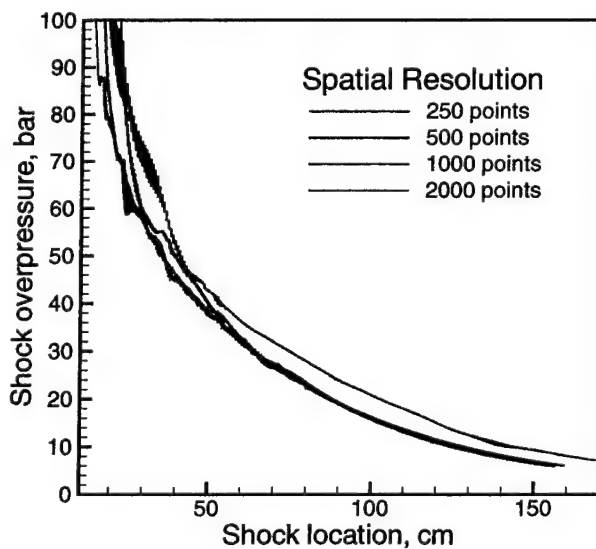
Figure 4: Effect of spatial resolution on pressure (a) and temperature (b). $R_b = 11$ cm, $W_{TNT} = 2.12$ kg. Cells = 2000 (solid) and 250 (dashed). $\Delta t = 0.05$ μs.

Figure 5: Effect of spatial resolution on shock location (a) and overpressure (b). $R_b = 11$ cm, $W_{TNT} = 2.12$ kg. $\Delta t = 0.05$ μs.
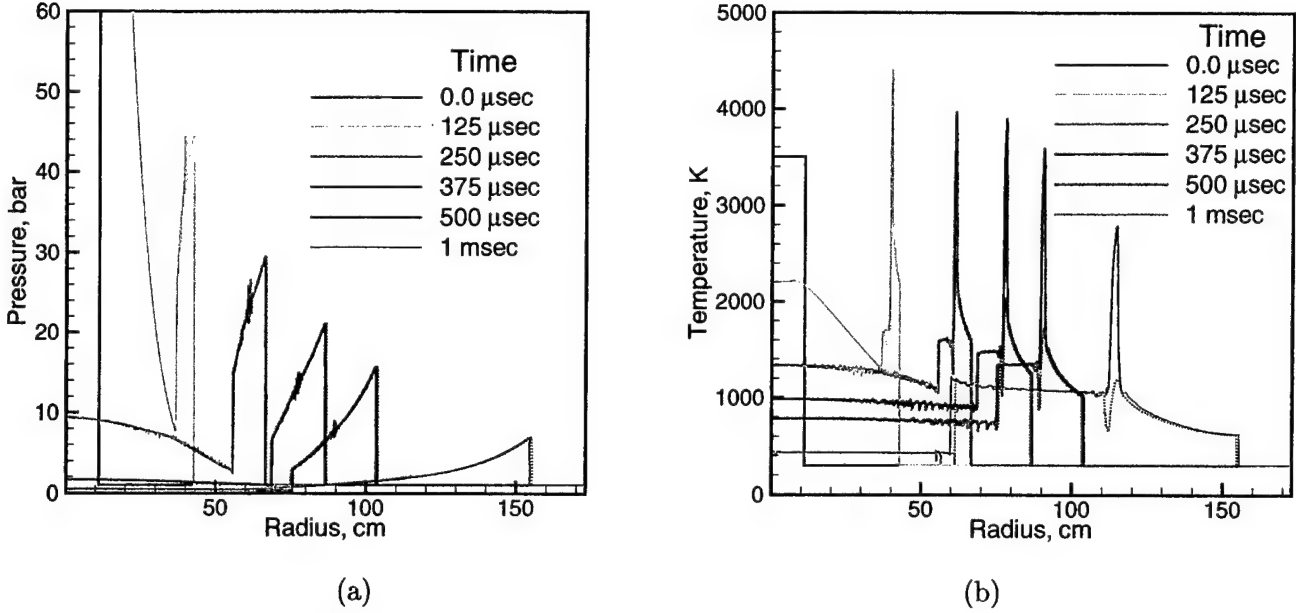
10

Figure 6: Effect of CO and C(s) reactions on pressure (a) and temperature (b). $R_b = 11$ cm, $W_{TNT} = 2.12$ kg. With (solid) and without (dashed) reactions. Cells = 2000. $\Delta t = 0.05$ μs.

density, and species densities can be slightly out of phase due to differing amounts of numerical diffusion.

Next, we examine the effect of blast radius on the pressure and temperature solutions (Figure 7), and on the shock location and shock overpressure (Figure 8). A suitable lower limit on the blast radius is the physical radius of the TNT, which is 6.75 cm for this simulation. An upper limit for the blast radius of 14.8 cm is chosen because that is the smallest radius where the ideal gas law is valid for the entire domain. The solution tends to be very sensitive to the initial blast radius used in the simulations. In particular, from Figure 8 it is apparent that the smaller radius gives much larger overpressures than the larger blast radii, due to the extreme increase in the initial pressures as the radius is reduced, as shown in Table 2. In addition, as the radius is reduced, the temperature and density after the contact discontinuity is reduced significantly, which is the result of much stronger expansion.

Finally, the spherically-symmetric one-dimensional case is compared with an axi-symmetric case. For the simulations, we choose $\Delta x = 0.346$ cm resolution (500 cells) because the differences in the solution between that and higher resolutions is small and we would like efficient axi-symmetric computations. The axi-symmetric geometry is 173 cm x 173 cm and has the same resolution (500 x 500 cells). Both cases use the 11.1 cm blast radius. The results are shown in Figure 9 and 10. Two things are important to note. First, the initial shock wave and pressure solution is almost exactly the same between the one-dimensional and axi-symmetric solutions. This suggests that mitigation studies done for the initial blast can be done adequately with the one-dimensional simulations. Second, the flame created at the contact discontinuity by the mixing of oxygen, carbon monoxide,
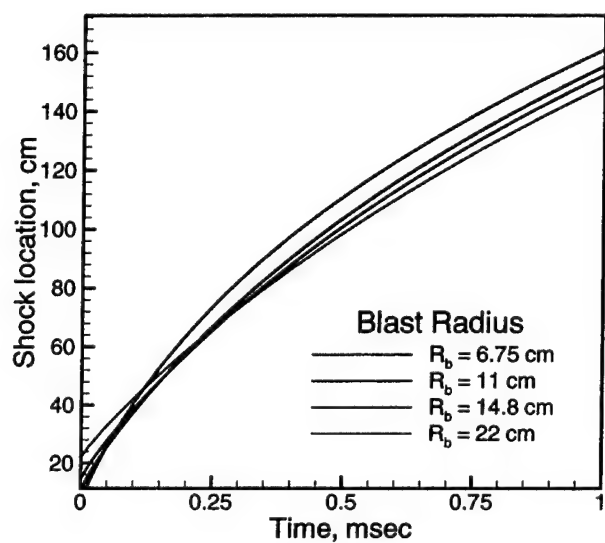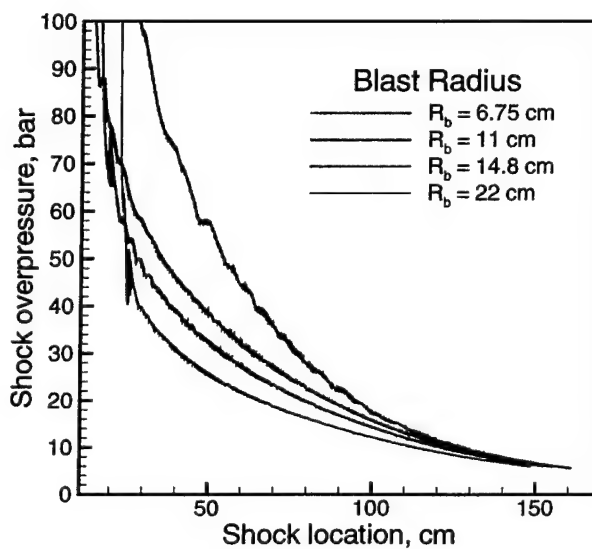
11
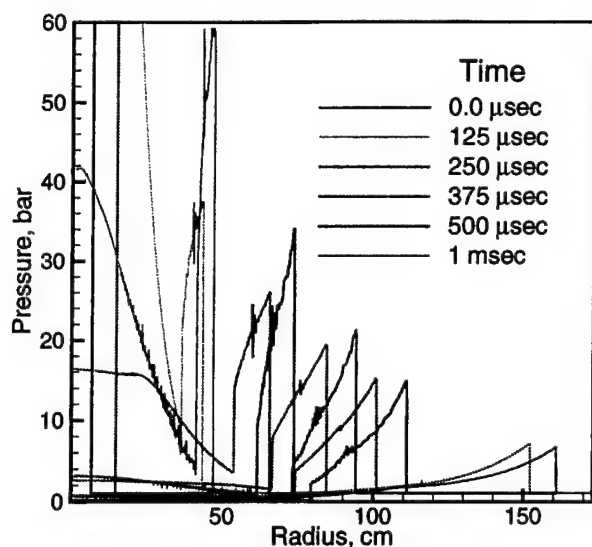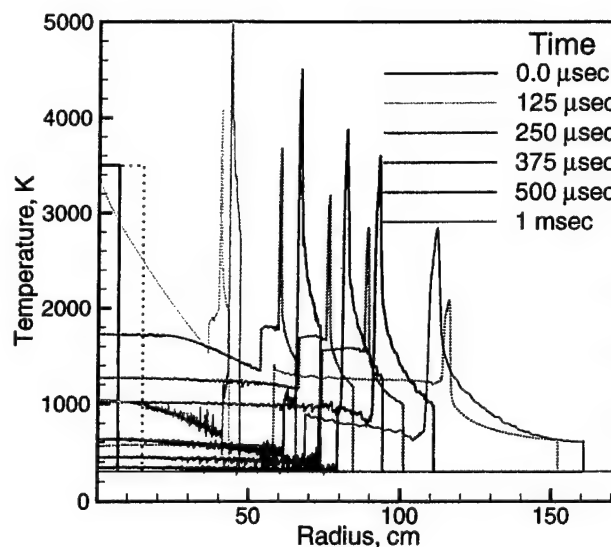
Figure 7: Effect of blast radius on pressure (a) and temperature (b). $W_{TNT} = 2.12$ kg. Cells = 2000. Blast radius $R_b = 6.75$ cm (solid) and $R_b = 14.8$ cm (dashed). $\Delta t = 0.05$ μs.

Figure 8: Effect of blast radius on shock location (a) and overpressure (b). $W_{TNT} = 2.12$ kg. Cells = 2000. $\Delta t = 0.05$ μs.
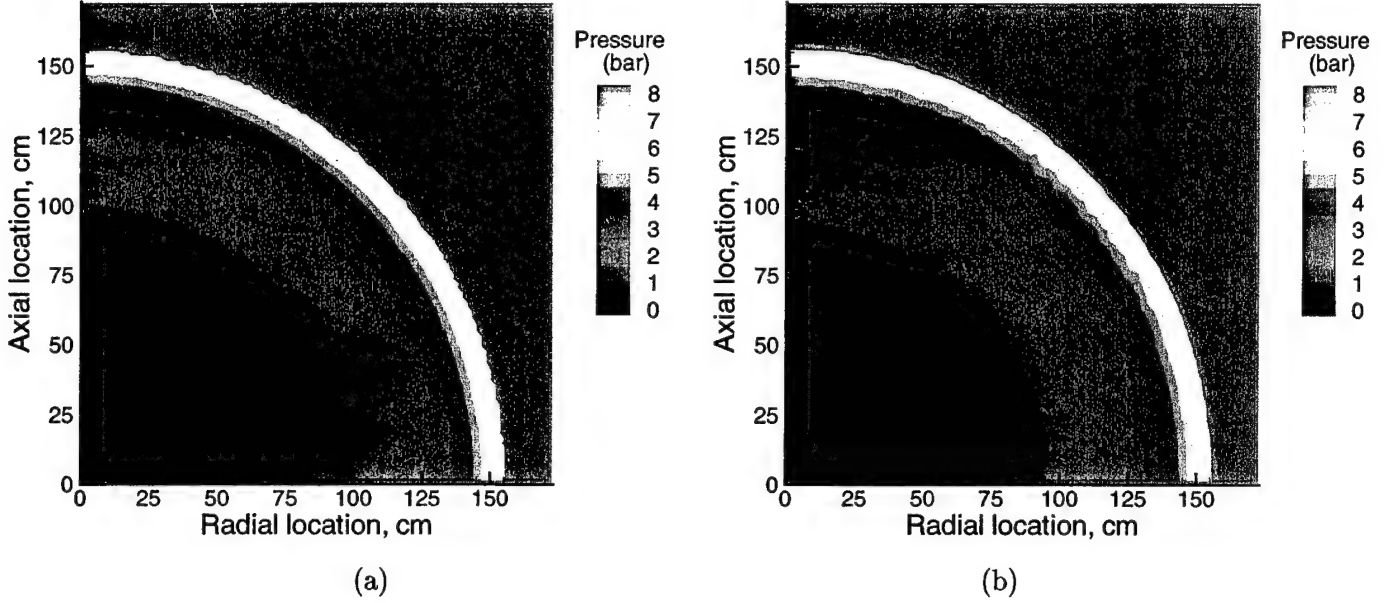
12

Figure 9: Comparison of one-dimensional (a) and axi-symmetric (b) pressure solutions. $R_b = 11$ cm, $W_{TNT} = 2.12$ kg. Cells = 500. $\Delta t = 0.25$ μs.

and carbon dust is unstable and tends to wrinkle. This wrinkling, although not terribly important for the initial shock, becomes important for quasi-steady simulations, as will be shown below.

It is important to compare these results with actual experimental data. Our first comparison for the one-dimensional spherical simulation is with data compiled by Kinney and Graham [13] on the peak overpressure of blasts, and is shown in Figure 11. We compare overpressures at six separate points within the domain, for three different blast radii. In addition, we consider $R_b = 6.75$ cm results both with and without the modified equation of state, as presented earlier. (The $R_b = 22$ cm results do not need the modified equation of state because the initial pressure is below 500 atm). We can see from this result that for comparisons with experiment, it is essential to use the 6.75 cm blast radius with a modified equation of state.

3.2   Quasi-steady simulations

In addition to the initial blast, the long term pressure developed in an enclosure is also of importance for mitigation. For the case of TNT, this overpressure is closely tied to the secondary fireball reactions instead of the initial blast pressure, because the majority of heat released from the explosive is part of the afterburn heat. To investigate this, a set of long time simulations were computed to obtain quasi-steady pressures for comparison with experimental data. These simulations involved shock reflections that often make the flow-field quite complex, and required at least an axi-symmetric simulation in order to correctly model the mixing that occurs due to turbulence.

For these simulations, we use an axi-symmetric domain with a radius of 173 cm and a length
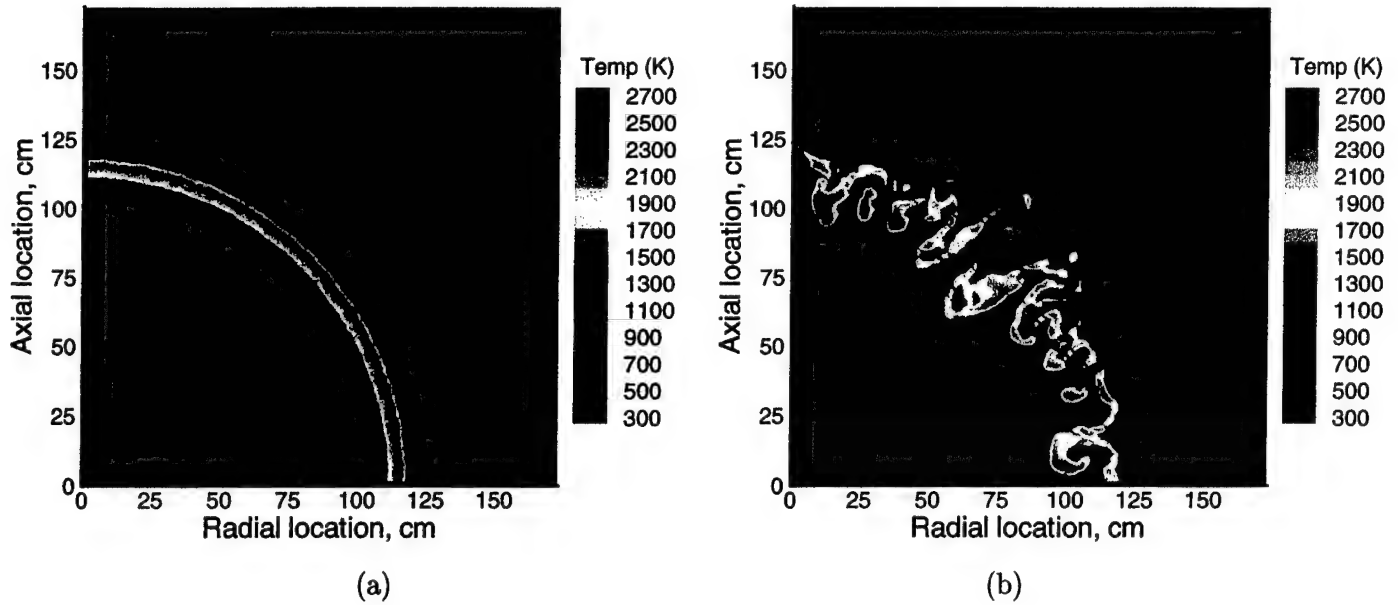
13

Figure 10: Comparison of one-dimensional (a) and axi-symmetric (b) temperature solutions. $R_b = 11$ cm, $W_{TNT} = 2.12$ kg. Cells = 500. $\Delta t = 0.25$ μs.
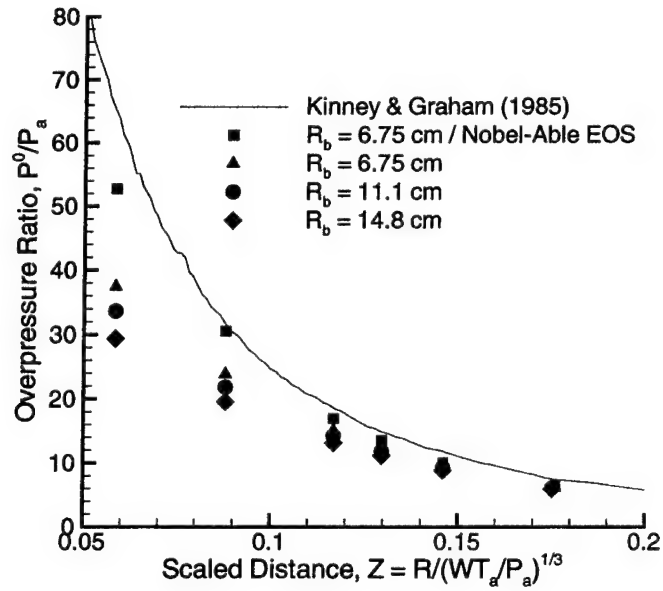

Figure 11: Comparison of peak overpressure with data compiled by Kinney and Graham (1985). Pressures are in bars, distance R is in meters, weight of charge W is in kilograms, and ambient temperature T_a is in Kelvins.
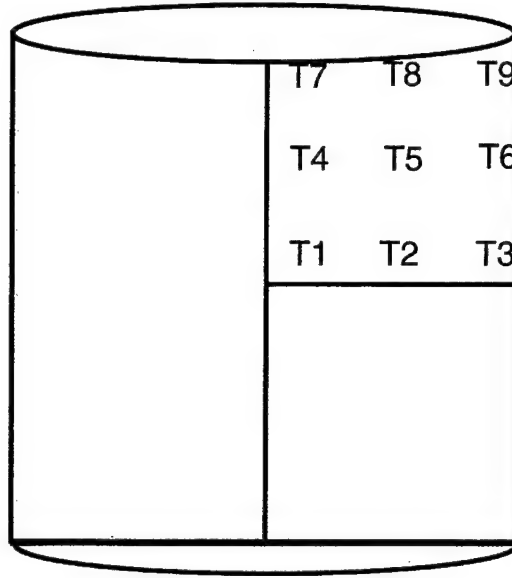
14

Figure 12: Geometry and pressure trace locations for axi-symmetric geometry. Station locations: 1) $r = 0.1$ cm, $z = 0.1$ cm, 2) $r = 86.5$ cm, $z = 0.1$ cm, 3) $r = 172.9$ cm, $z = 0.1$ cm, 4) $r = 0.1$ cm, $z = 86.5$ cm, 5) $r = 86.5$ cm, $z = 86.5$ cm, 6) $r = 172.9$ cm, $z = 86.5$ cm, 7) $r = 0.1$ cm, $z = 172.9$ cm, 8) $r = 86.5$ cm, $z = 172.9$ cm, 9) $r = 172.9$ cm, $z = 172.9$ cm

of 346 cm. Using symmetry arguments, our computational domain is 173 cm x 173 cm. For comparison, we also compute a spherically-symmetric one-dimensional solution with a radius of 198 cm, chosen such that the volume of the sphere and the cylinder are the same as the NCEL test results [14]. The grid size for the axi-symmetric geometry is 500 x 500, chosen such that we have a fairly efficient calculation without sacrificing much accuracy. For the axi-symmetric calculations, we take pressure traces at nine locations within the domain, as shown in Figure 12. For these simulations we use a spherical blast radius of 11 cm for both the one-dimensional and axi-symmetric simulations, centered at $r = 0$ cm, $z = 0$ cm (near station 1 at the center of the cylinder).

The first results shown are comparisons of pressure between the one-dimensional computation (pressure trace taken at $r = 100$ cm) and station 5 of the axi-symmetric simulation. The pressures are plotted in psig for easy comparison with experimental data. The first noticeable feature of this plot is the distinct difference between the one-dimensional and axi-symmetric results. There are two main reasons for this. First, because of the spherical geometry, the main shock will tend to only bounce back and forth within the domain and never create complex reflection patterns such as in the multi-dimensional cases. Additionally, by forcing spherical symmetry, the instabilities seen in Figure 10 will not develop. Both of these features restrict the development of turbulence and inhibit the mixing between CO, C(s), and oxygen, resulting in much of the secondary fireball energy not being released as quickly as in the axi-symmetric and experimental cases.

The second noticeable feature of this plot is the quasi-steady pressure seen in the axi-symmetric case compared with the experimental cases. The axi-symmetric case is quite a bit higher than the
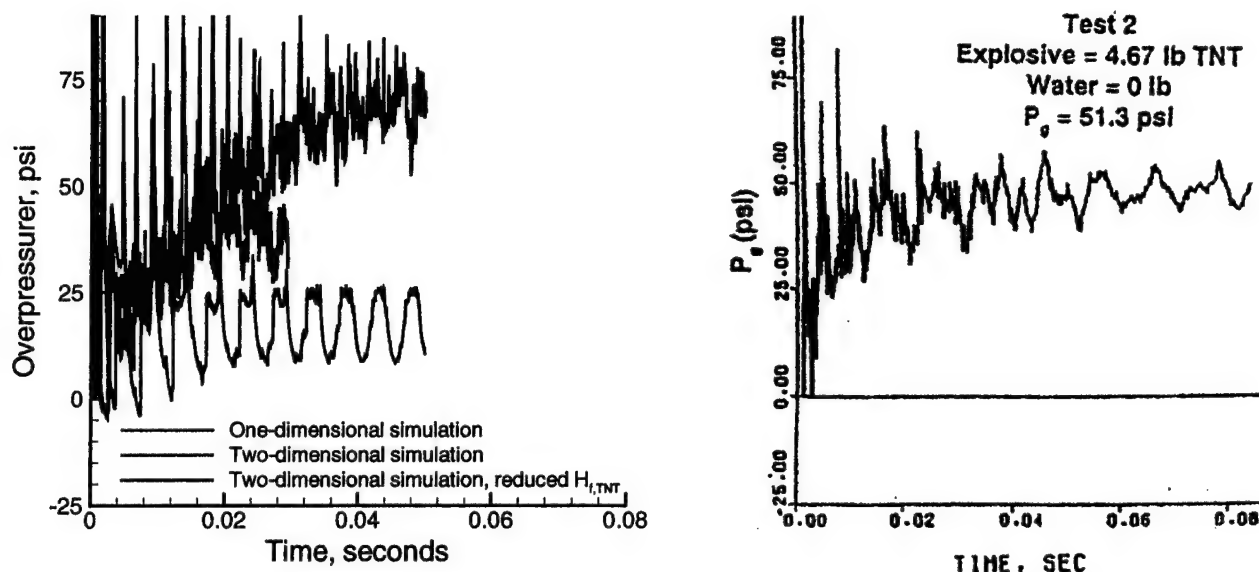
Figure 13: Pressure traces in center of domain for one-dimensional and two-dimensional quasi-steady simulations. $R_b = 11$ cm, $W_{TNT} = 2.12$ kg. Cells $= 500$. $\Delta t = 0.25$ μs.

experimental case. There are several reasons for this. First of all, there is uncertainty associated with the heat of formation of TNT. For the initial blast results, we found that the higher heats of formation compared much better with the results of Kinney and Graham for the initial blast. However, these values may need to be adjusted for the quasi-steady calculations. Also, the simulations assume everything reacts completely; however, in reality, for high-temperature flames many species will reach an equilibrium and not fully react, while other species will tend to dissociate. Both of these processes tend to drive the flame temperature (and thus the pressure developed within the enclosure) down toward the experimental enclosure pressure.

The next result shown is pressure and temperature snapshots at 5 ms, 10 ms, and 50 ms for the axi-symmetric domain (Figure 14). All of these snapshots occur after the initial blast wave has reflected off the outer wall. The most important thing to note from these snapshots is the incredibly complex nature of the solution after the initial shock reflection (compare these solutions with Figs. 9 and 10). This is especially true in terms of the temperature solution, where the initial instabilities in the contact discontinuity seen in Figure 10 have interacted with the reflected shock in a very complicated manner. Two additional points can be seen from these plots. First, the high temperature region, hindered partially by the reflected shock waves, takes a significant amount of time (relative to the initial blast) to get to the outer wall. Second, the pressure solution shows strong spatial variation at least 10 ms after the initial blast, and perhaps for much longer. By about 50 ms, though, the pressure has evened out considerably within the chamber. This is due to the high amount of dissipation within the flow caused by the small scale structures.

Finally, Figure 15 shows pressure traces at each of the stations for the axi-symmetric solution. The interesting aspect of the different pressure traces is how different all of them are. All of the traces near the centerline are extremely noisy, which is believed to be a numerical artifact due
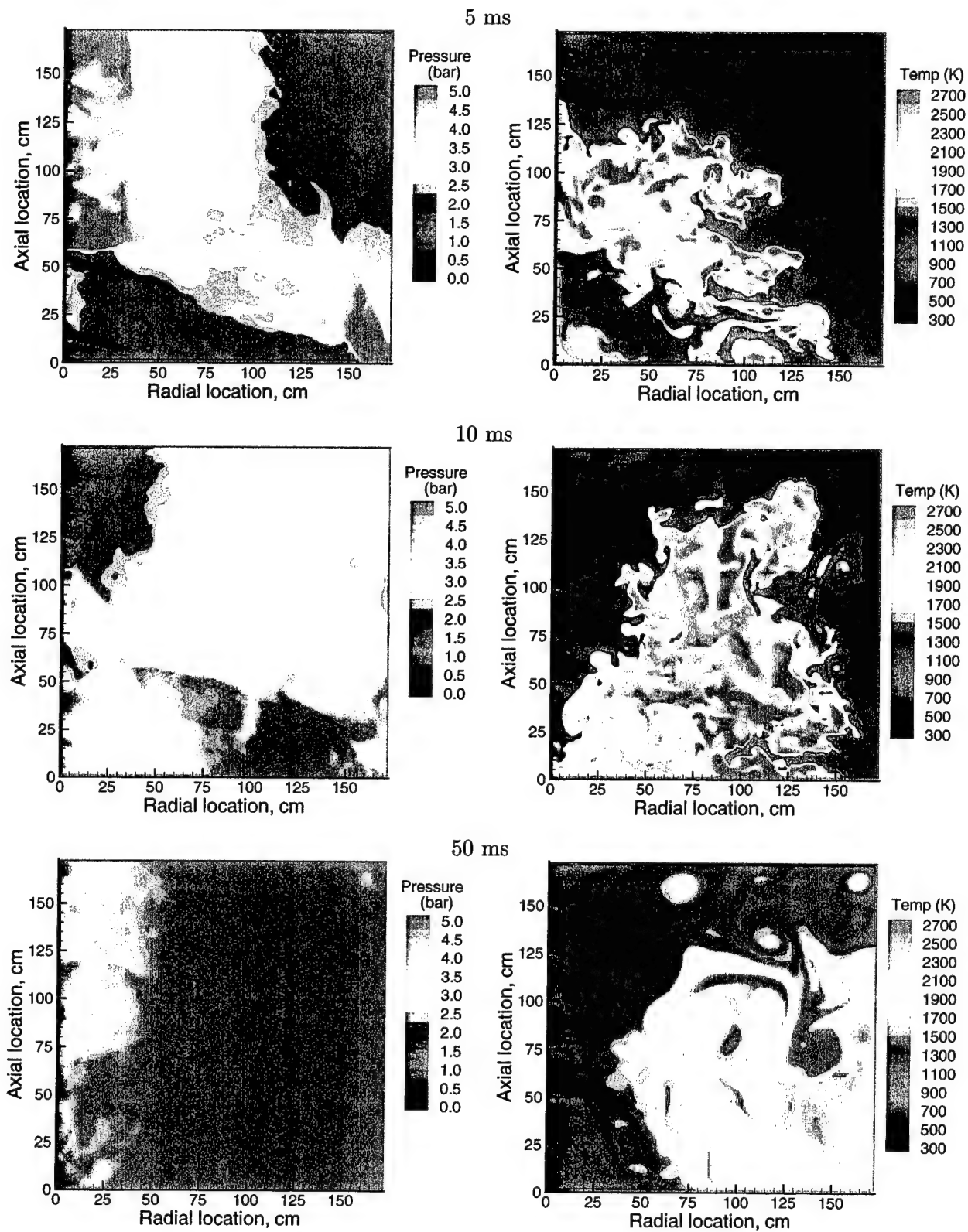
5 ms

10 ms

50 ms

Figure 14: Pressure (left) and temperature (right) solutions for two-dimensional case after 5 ms (top), 10 ms (middle), and 50 ms (bottom). $R_b = 11$ cm, $W_{TNT} = 2.12$ kg. Cells = 500. $\Delta t = 0.25$ μs.

to the extremely small cell sizes. All of the stations near the boundary also are more noisy than the central station (Station 5). Further investigation should be done to determine if this is just a numerical artifact or if there are physical reasons for this. Also, the quasi-static pressure is reached by about 30 ms, which corresponds nicely to experimental results.

4 Conclusions

This report has focused on our efforts to capture the two main features of explosions that we are interested in mitigating using water mist. The first feature is the initial blast overpressure. By selecting suitable initial conditions and appropriate thermo-chemical properties, we can predict shock overpressures to within 5% of experimental results for several locations within the simulation domain, without doing a detailed and expensive computation of the initial detonation within the explosive. We found that correct overpressure calculations do require the use of a modified gas equation of state; for these computations, we used the Nobel-Able gas law. Effective simulations of the initial blast overpressure were done using a spherically-symmetric one-dimensional solution procedure. Additional studies were done to determine the effect of resolution, afterburn reactions, and "blast" radius on the shock overpressures.

The second feature of interest is the quasi-steady pressure developed within the enclosure. This pressure is dependent on heat released in the secondary fireball reactions of carbon dust and carbon monoxide being oxidized to carbon dioxide. Multi-dimensional simulations were necessary to accurately predict the development of this overpressure due to mixing generated by complex shock reflections and instabilities within the contact surface that are present in multi-dimensional simulations, but absent in one-dimensional simulations. It was found that a slight adjustment of the heat of formation for TNT was necessary such that equilibrium chemistry and dissociation could be accounted for in the simple chemistry model to give the correct quasi-steady overpressure.

Additional studies will concentrate on developing water-mist models for examining the mitigation of the initial blast, and then the quasi-steady pressure and temperature within confined enclosures. Additionally, more simulations are needed for other explosives to determine the properties of the initial blast and quasi-steady pressure rise, and finally to determine the effectiveness of mitigation. Simulations will be done for room sized enclosures and also for more complicated geometries that are similar to geometries found aboard ships.
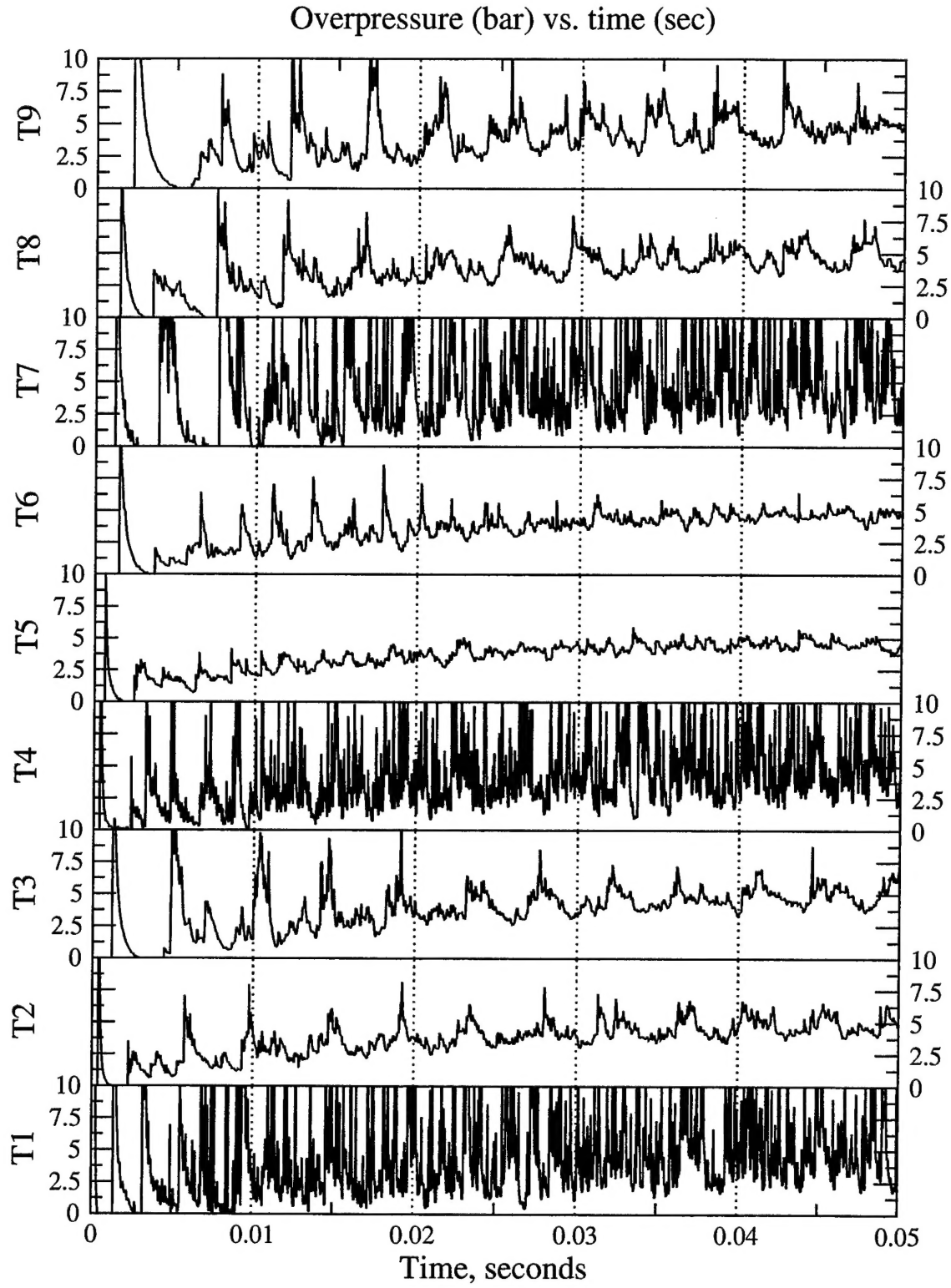
Overpressure (bar) vs. time (sec)

Figure 15: Pressure traces at selected points in the axi-symmetric domain as a function of time. $R_b = 11$ cm, $W_{TNT} = 2.12$ kg. Cells = 500. $\Delta t = 0.25$ μs.

19

References

[1] R.L. Darwin and F.W. Williams. The development of water mist fire protection systems for US Navy ships. *Naval Engineers J.*, 112(6):49–57, 2000.

[2] K. Kailasanath, P.A. Tatem, F.W. Williams, and J. Mawhinney. Blast mitigation using water— A status report. Technical Report NRL/MR/6410-02-8606, Naval Research Lab, 2002.

[3] K. van Wingerden. Mitigation of gas explosions using water deluge. *Process Safety Progress*, 19(3):173–178, 2000.

[4] G.O. Thomas. On the conditions required for explosion mitigation by water sprays. *Trans IChemE*, 78(B):339–354, 2000.

[5] P.W. Cooper. *Explosives Engineering*. Wiley-VCH, New York, NY, p. 131, 1996.

[6] F.E. Marble. Dynamics of dusty gases. *Annual Review of Fluid Mechanics*, 2:397–446, 1970.

[7] P.W. Cooper. *Explosives Engineering*. Wiley-VCH, New York, NY, p. 156, 1996.

[8] J.P. Boris and D.L. Book. Flux Corrected Transport I. SHASTA, A fluid transport algorithm that works. *J. Comput. Phys.*, 11(1):38–69, 1973.

[9] J.P. Boris, A.M. Landsberg, E.S. Oran, and J.H. Gardner. LCPFCT—A Flux-Corrected Transport algorithm for solving generalized continuity equations. Technical Report NRL/MR/6410-93-7192, Naval Research Lab, 1993.

[10] S. Gordon and B.J. McBride. Computer program for calculation of complex chemical equilibrium compositions, rocket performance, incident and reflected shocks and Chapman-Jouquet detonations. Technical Report NASA Report SP-273, NASA, 1971.

[11] K. Prasad, G. Patnaik, and K. Kailasanath. Advanced simulation tool for improved damage assessment 1) a multiblock technique for simulating fire and smoke spread in large complex enclosures. Technical Report NRL/MR/6410-00-8428, Naval Research Lab, 2000.

[12] K. Prasad, C. Li, K. Kailasanath, C. Ndubizu, R. Ananth, and P. Tatem. Numerical modeling of fire suppression using water mist. 1. gaseous methane-air diffusion flames. Technical Report NRL/MR/6410-98-8102, Naval Research Lab, 1998.

[13] G.F. Kinney and K.J. Graham. *Explosive Shocks in Air*. Springer-Verlag, Berlin, 1985.

[14] W.A. Keenan and P.C. Wager. Mitigation of confined explosion effects by placing water in proximity of explosives. In *25th DoD Explosives Safety Seminar*, Anaheim, CA, August 18-20 1992.

A Thermodynamic curve-fits

The thermodynamic data for each gas species is shown below. It is arranged such that for each species, the first line states the formula name, phase, molecular weight, and the temperature ranges of the thermodynamic curve-fits, and the subsequent lines are the coefficients for the thermodynamic curve-fits. Most species have a low temperature curve-fit and a high temperature curve-fit. Numbering the coefficients for each temperature range a_1 to a_7, the specific heat (C_p) is calculated as:

$$\frac{C_p}{R} = \sum_{n=1}^{5} a_n T^{n-1} \tag{13}$$

The enthalpy is calculated using the relation $h(T) = \int_{T_{ref}}^{T} C_p(T)\, dt + h_{ref}$:

$$\frac{h}{RT} = \sum_{n=1}^{5} \frac{a_n T^{n-1}}{n} + \frac{a_6}{T} \tag{14}$$

Entropy is calculated using the relation $s^o(T) = \int_{T_{ref}}^{T} C_p(T)/T\, dT + s^o_{ref}$:

$$\frac{s^o}{R} = a_1 \ln T + \sum_{n=2}^{5} \frac{a_n T^{n-1}}{n-1} + a_7 \tag{15}$$

```
therm.dat
 C7H5N3O6           crystal  227.13       300.  5000.
  29.26000 0.0000000E-00 0.0000000E-00 0.0000000E-00 0.0000000E-00 -8778.000 0.000000
 O2                 gas      31.9988003   300.  1000.  5000.
   3.212936 0.1127486E-02 -.5756150E-06 0.1313877E-08 -.8768554E-12 -1005.249 6.034738
   3.697578 0.6135197E-03 -.1258842E-06 0.1775281E-10 -.1136435E-14 -1233.930 3.189166
 H2O                gas      18.0153401   300.  1000.  5000.
   3.386842 0.3474982E-02 -.6354696E-05 0.6968581E-08 -.2506588E-11 -30208.11 2.590233
   2.672146 0.3056293E-02 -.8730260E-06 0.1200996E-09 -.6391618E-14 -29899.21 6.862817
 CO                 gas      28.0105505   300.  1000.  5000.
   3.262452 0.1511941E-02 -.3881755E-05 0.5581944E-08 -.2474951E-11 -14310.54 4.848897
   3.025078 0.1442689E-02 -.5630828E-06 0.1018581E-09 -.6910952E-14 -14268.35 6.108218
 CO2                gas      44.0099506   300.  1000.  5000.
   2.275725 0.9922072E-02 -.1040911E-04 0.6866687E-08 -.2117280E-11 -48373.14 10.18849
   4.453623 0.3140169E-02 -.1278411E-05 0.2393997E-09 -.1669033E-13 -48966.96 -.9553959
 N2                 gas      28.0133991   300.  1000.  5000.
   3.298677 0.1408240E-02 -.3963222E-05 0.5641515E-08 -.2444855E-11 -1020.900 3.950372
   2.926640 0.1487977E-02 -.5684761E-06 0.1009704E-09 -.6753351E-14 -922.7977 5.980528
 C(S)               crystal  12.0111504   300.  1000.  5000.
  -.6705661 0.7181500E-02 -.5632921E-05 0.2142299E-08 -.4168562E-12 -73.39498 2.601596
   1.490166 0.1662126E-02 -.6687204E-06 0.1290880E-09 -.9205334E-14 -707.4019 -8.717785
```